


# Optical storage of circular airy beam in atomic vapor

Hong Chang(常虹), Xin Yang(杨欣), Yan Ma(马燕), Xinqi Yang(杨鑫琪), Mingtao Cao(曹明涛), Xiaofei Zhang(张晓斐), Ruifang Dong(董瑞芳), and Shougang Zhang(张首刚)

**Citation:**Chin. Phys. B, 2024, 33 (**8**): 084202. DOI: 10.1088/1674-1056/ad4bbf

**What follows is a list of articles you may be interested in**

---

## Wavelength-interval switchable Brillouin-Raman random fiber laser through Brillouin pump manipulation

Yang Li(李阳), En-Ming Xu(徐恩明), Rui-Jia Chen(陈睿佳), Yu-Gang Shee, and Zu-Xing Zhang(张祖兴)

Chin. Phys. B, 2024, 33 (**7**): 074209. DOI: 10.1088/1674-1056/ad3efb

## Broadband bidirectional Brillouin-Raman random fiber laser with ultra-narrow linewidth

Qian Yang(杨茜), Yang Li(李阳), Hui Zou(邹辉), Jie Mei(梅杰), En-Ming Xu(徐恩明), and Zu-Xing Zhang(张祖兴)

Chin. Phys. B, 2024, 33 (**2**): 024206. DOI: 10.1088/1674-1056/ad09cb

## Ultraviolet metalens and metalens array of focused vortex beams

Jinping Zhang(张金平), Yan Wang(王焱), Huan Yuan(袁欢), Zehao Wang(王泽豪), Yang Deng(邓阳),Chengzhi Huang(黄承志), Jiagui Wu(吴加贵), and Junbo Yang(杨俊波)

Chin. Phys. B, 2023, 32 (**6**): 064206. DOI: 10.1088/1674-1056/ac9d87

## Unconventional phase transition of phase-change-memory materials for optical data storage

Nian-Ke Chen(陈念科), Xian-Bin Li(李贤斌)

Chin. Phys. B, 2019, 28 (**10**): 104202. DOI: 10.1088/1674-1056/ab3cc3

## Experimental study of the dependences of retrieval efficiencies on time delay between magneto-optical-trap being turned off and optical storage

Li-Rong Chen(陈力荣), Zhong-Xiao Xu(徐忠孝), Ping Li(李萍), Ya-Fei Wen(温亚飞), Wei-Qing Zeng(曾炜卿), Yue-Long Wu(武跃龙), Long Tian(田龙), Shu-Jing Li(李淑静), Hai Wang(王海)

Chin. Phys. B, 2016, 25 (**2**): 024203. DOI: 10.1088/1674-1056/25/2/024203

---

# Optical storage of circular airy beam in atomic vapor

Hong Chang(常虹)[1,2], Xin Yang(杨欣)[3], Yan Ma(马燕)[1,2], Xinqi Yang(杨鑫琪)[1,2], Mingtao Cao(曹明涛)[1,2,†], Xiaofei Zhang(张晓斐)[4], Ruifang Dong(董瑞芳)[1,2,5,‡], and Shougang Zhang(张首刚)[1,2,§]

[1] *Key Laboratory of Time Reference and Applications, National Time Service Center, Chinese Academy of Sciences, Xi'an* 710600, *China*
[2] *School of Astronomy and Space Science, University of Chinese Academy of Sciences, Beijing* 100049, *China*
[3] *Ministry of Education Key Laboratory for Nonequilibrium Synthesis and Modulation of Condensed Matter, Shaanxi Province Key Laboratory of Quantum Information and Quantum Optoelectronic Devices, School of Physics, Xi'an Jiaotong University, Xi'an* 710049, *China*
[4] *Department of Physics, Shaanxi University of Science and Technology, Xi'an* 710021, *China*
[5] *Hefei National Laboratory, Hefei* 230088, *China*

(Received 19 February 2024; revised manuscript received 27 April 2024; accepted manuscript online 15 May 2024)

The realization of quantum storage of spatial light field is of great significance to the construction of high-dimensional quantum repeater. In this paper, we experimentally realize the storage and retrieval of circular Airy beams (CABs) by using the $\Lambda$-type three-level energy system based on the electromagnetically induced transparency in a hot rubidium atomic vapor cell. The weak probe beam field is modulated with phase distribution of CABs by a spatial light modulator. We store the probe circular Airy beam (CAB) into the rubidium atomic vapor cell and retrieve it after the demanded delay. We quantitatively analyze the storage results and give corresponding theoretical explanations. Moreover, we investigate the autofocusing and self-healing effect of the retrieved CAB, which indicates that the properties and beam shape of CAB maintain well after storage. Our work will have potential applications in the storage of high-dimensional quantum information, and is also useful for improving the channel capacities of quantum internet.

**Keywords:** circular Airy beam, optical storage, autofocusing effect, self-healing effect

**PACS:** 42.60.Jf, 42.25.Bs, 32.80.Qk, 42.50.Gy **DOI:** 10.1088/1674-1056/ad4bbf

## 1. Introduction

Circular Airy beams (CABs) have attained much attention because of their abruptly autofocusing property,[1–3] which were first proposed in 2010[1] and investigated by experiment in 2011.[2,3] Due to the self-bending property of Airy beam,[4,5] the circular Airy beam (CAB) will suddenly autofocus in the focal region. The energy flows from the main ring to the center of CAB. Therefore, the autofocusing property of CAB has been widely used in optical tweezers,[6–9] light bullet,[10–12] atom manipulation[13,14] and quantum information.[15–17]

Studies on the self-bending behavior of the Airy beam show that its parabolic trajectory is controllable[18–20] by changing the initial incidence angle of Airy beams[18] or the refractive index gradient of the medium.[20] Moreover, the manipulation of the Airy beams' deflection position by changing the Rabi frequencies of the control beam in the atomic vapor with the electromagnetically induced transparency (EIT) scheme has been theoretically proposed by Zhuang *et al.*[21] Later, manipulating the Airy beams between atom–light interface has attracted much attention.[21–26] In the atomic system, the manipulation of the self-accelerating beams' propagation properties can be realized in the EIT scheme,[21–23] which can be extended to two-dimensional[23,25] and three-dimensional[26] self-accelerating beams. The EIT protocol also presents the possibility to store the Airy beam to the atomic medium, which has potential applications in the storage of high-dimensional quantum information.

Principally, the storage of CAB can be realized by different quantum memory protocols, such as, the Duan–Lukin–Cirac–Zoller protocol,[27] EIT protocol,[28–31] photo-echo protocol,[32,33] and Raman protocol.[34,35] Among these protocols, EIT has been selected as the most popular candidate to store spatial mode information.[22,36–38] The storage of Airy wave packets has been theoretically investigated in the EIT-driven atomic gas by Hang *et al.*[22,36] Then, the storage of 2D Airy wave packet experimentally demonstrated in a doped solid EIT-driven by Wang *et al.*[37] and in atomic vapor by Wang *et al.*[38] However, the storage of CAB has not yet been investigated experimentally, which is essentially important because of the abruptly autofocusing property in atomic medium that could be employed to present the waveguided multiplexed quantum memory.

In this paper, we experimentally investigate the storage of CAB in a hot atomic vapor with EIT scheme. The experimental results show that the autofocusing and self-healing effect of the retrieved CAB can be well preserved. Our results will be useful for high-dimensional spatial multi-

†Corresponding author. E-mail: mingtaocao@ntsc.ac.cn
‡Corresponding author. E-mail: dongruifang@ntsc.ac.cn
§Corresponding author. E-mail: szhang@ntsc.ac.cn

© 2024 Chinese Physical Society and IOP Publishing Ltd 

modes storage and high-dimensional quantum information communication.[15,16,39–44]

## 2. Theoretical analysis

The electric field of CAB at the initial plane is expressed as[1,44,45]

$$u(x,y,z=0) = \mathrm{Ai}\left(\frac{r_0-\sqrt{x^2+y^2}}{b\cdot\omega}\right) \times \exp\left(a\cdot\frac{r_0-\sqrt{x^2+y^2}}{b\cdot\omega}\right), \quad (1)$$

where $(x, y)$ is the Cartesian coordinate system, Ai is the Airy function, and its expression is

$$\mathrm{Ai}(x) = \frac{1}{\pi}\int_0^{\infty}\cos\left(\frac{1}{3}t^3+xt\right)\mathrm{d}t.$$

The $t$ means the variable of integration.[46] $r_0$, $\omega$ and $b$ are respectively the radius of the main ring, the radial width, and the distribution factor of CAB in the initial plane. $a$ is a decay factor.

As shown in Fig. 2, the CAB consists of several rings at the initial image plane. The CAB possesses abruptly autofocusing property because of the characteristics of the Airy function. The radius of the main ring of CAB also follows a parabolic trajectory before reaching its focus.[2,18] The focal position $z_f$ is defined as[47]

$$z_f = 4\pi\frac{b\omega}{\lambda}\sqrt{r_0\omega}, \quad (2)$$

where $\lambda$ is the wavelength, which is 795 nm in this paper. Herein, the light power is 630 μW, the other parameters are $r_0 = 0.5$ mm, $a = 0.1$, $b = 0.022$, $\omega = 2$ mm. Then we can calculate this CAB will autofocus at $z_f = 695$ mm.

## 3. Experimental configuration

The schematic experimental setup is depicted in Fig. 1. In Fig. 1(a), the two laser beams respectively from the laser 1 (EFL-SSHG-795-DFB) and laser 2 (EFL-SSHG-795-FECL) are defined as the probe and control beams. After the two beams of the laser 1 and laser 2 pass through the single-mode fiber to improve the spatial mode, they are frequency shifted by the acousto-optic modulator (AOM), as shown in Fig. 1(c). It is well known that Airy wave packets can be generated via the Fourier transformation of a Gaussian beam modulated with a cubic phase.[48] Thus, Airy beam becomes a CAB in polar coordinates. In our experiments, a spatial light modulator (SLM, HDSLM80R Plus) is utilized to generate a CAB, which is defined as the probe beam with a power of 630 μW and a diameter of 2 mm. A beam splitter (BS) is used to separate the probe beam into two beams, and one of them is defined as the reference beam. Meanwhile, a telescope consisting of $f_3$ and $f_4$ is used to expand the control beam size and the achieved high-quality Gaussian beam is about 4 mm in diameter. A 70 mm long $^{85}$Rb atomic gas cell is placed in a three-layer μ-metal magnetic shield and is set to 55 °C with a temperature controller. Finally, the probe and control beams are injected into the hot rubidium cell in the same direction.

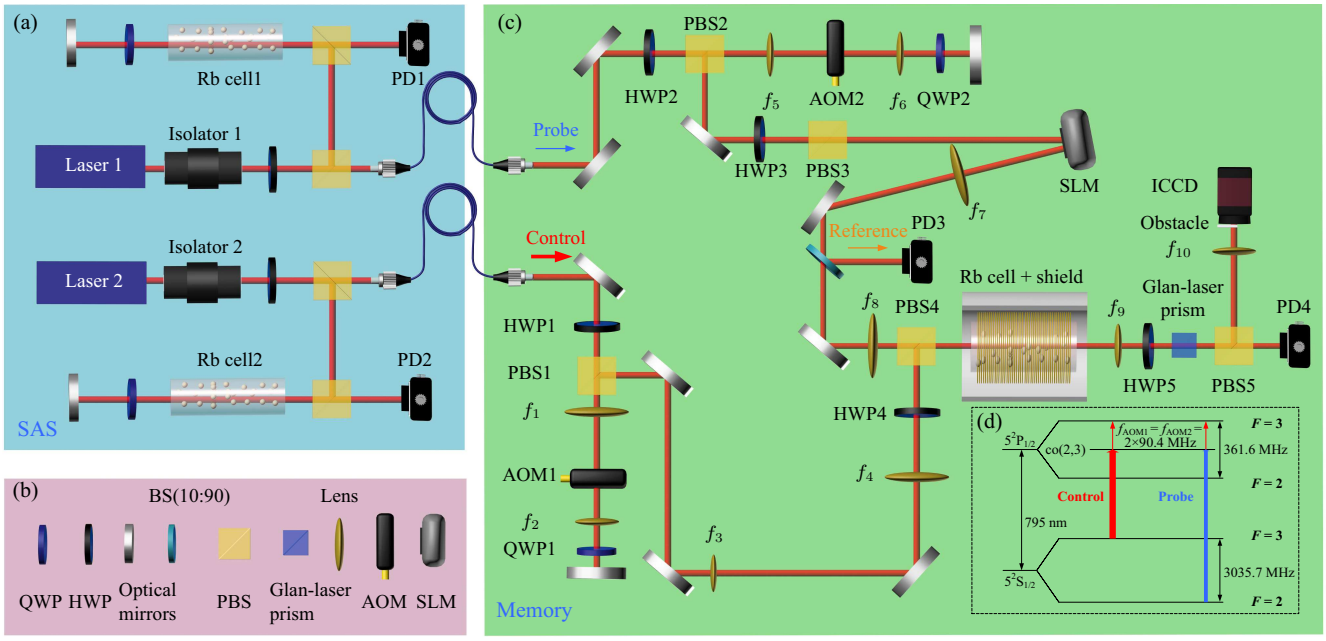



**Fig. 1.** (a) The saturated absorption spectroscopy (SAS) system. (b) The optical elements in the experiment. (c) The experimental setup of the storage of CAB. (d) The detailed three-level coupled system for EIT storage in a hot $^{85}$Rb atomic gas cell. (QWP, quarter-wave plate; HWP, half-wave plate; BS, beam splitter; PBS, polarizing beam splitter; AOM, acousto-optic modulator; SLM, spatial light modulator; $f_1$, $f_3$ and $f_4$, lenses with the focal length of $f = 100$ mm, 50 mm and 300 mm; $f_2$, $f_5$ and $f_6$, lenses with the same focal length of $f = 75$ mm; $f_7$ and $f_8$, lenses with the same focal length of $f = 500$ mm; $f_9$ and $f_{10}$, lenses with the same focal length of $f = 200$ mm; PD, photodiode detector; ICCD, intensified charge coupled device.)

The energy level structure is as shown in Fig. 1(d). The 795 nm probe laser is frequency-locked to the $^{85}$Rb D1 line with the crossover transition $5^2S_{1/2}, F = 2 \rightarrow 5^2P_{1/2}, F' = 2$, 3, which is depicted as the co(2,3) in Fig. 1(d). The control laser is phase-locked to the probe laser and is resonant with the crossover transition $5^2S_{1/2}, F = 3 \rightarrow 5^2P_{1/2}, F' = 2$, 3. The experimental parameters of the two beams can be controlled independently. These two beams form a typical $\Lambda$-type EIT system to perform the experiment.

In the experiment, the beams from laser 1 and laser 2 pass through the double-pass AOM, and then the frequencies of both probe and control beams are shifted by 180.8 MHz. Thus, the probe and control beams are resonant with the $5^2S_{1/2}, F = 2 \rightarrow 5^2P_{1/2}, F' = 3$ transition and the $5^2S_{1/2}, F = 3 \rightarrow 5^2P_{1/2}, F' = 3$ transition, respectively. The probe beam with the horizontally polarized is imaged to the center of the cell by a $4f$ system with $f_7$ and $f_8$, as depicted in Fig. 1(c). A circular aperture is positioned at the focal plane of the $4f$ system to act as a filter, selecting the zero-order diffracted spot of CAB appearing in the Fourier plane. After the SLM, the reflected beam passes through the Fourier transform lens $f_8$ to observe the CAB profile at the focal point of the $f_8$. The reference beam is directly coupled on the photodiode detector (PD, Thorlabs PDA8A2). The size of vertically polarized control beam, with a power of 60 mW, completely covers the probe CAB. And it propagates collinearly with the probe beam through the polarizing beam splitter (PBS4) and is reflected through PBS5. By adjusting HWP5 and PBS5, the probe beam passing through the hot gas cell can be detected by ICCD or PD. In one case, the probe beam after the cell is sent to another $4f$ system with $f_9$ and $f_{10}$ and then is detected by an intensified charge-coupled device (ICCD, iStar 334T) to record the spatial intensity profile of CAB. In the other case, the probe beam is sent to a PD to record the pulse profile in the time domain.

## 4. Experimental results and discussion

### 4.1. The propagation characteristics of CAB before storage

The results of spatial intensity distribution of CAB as shown in Fig. 2. The CAB can be visualized as the result of a one-dimensional Airy beam at a radial position being rotated around the center of the circle. Therefore, CABs could abruptly autofocus at the focal region. The autofocusing ability of CAB is verified in free space. The ICCD is initially placed at the focal plane of $f_{10}$, and $z_1$ represents the distance between the focal plane of $f_{10}$ and the ICCD. It can be seen from Fig. 2(a) that the intensity distribution of CAB beam forms a hollow ring in the initial plane. To obtain Fig. 2(c), we calculated the normalized intensity distribution of the red dotted section located at $z_1 = 0$ mm in Fig. 2(a). The light intensity at the center of CAB is zero and the intensity of the first main ring of the CAB takes up most of the light intensity. And the intensity profiles are shown in Fig. 2(c). As the CAB is transmitted, the size of the main ring gradually decreases. As the energy flows to the main ring, the transmission distance $z_1$ increases. In Fig. 2(c), when $z_1 = 450$ mm, the tallest and relatively narrow peak appears at the center of $x$-axis. And then, the peak at the center of $x$-axis becomes narrower when $z_1$ increases from 450 mm to 700 mm. As shown in Fig. 2(e), the full width at half maximum (FWHM) of the autofocusing process of CAB in free space decreases from 1.07 mm to 0.36 mm, indicating that the CAB has almost become a solid spot.

By placing an opaque rectangular obstacle at the focal plane of $f_{10}$ to block most of the main ring of CAB, we demonstrate the self-healing property of CAB by moving the ICCD. Figure 2(b) shows the experimental results of the self-healing process of CAB for different $z_2$ values, where $z_2$ is the distance between the obstacle and ICCD. Because the obstacle is placed at $z_2 = 0$ mm, the initial $z_2$ is set to 25 mm from the image plane. Figure 2(d) is obtained by using the same method as Fig. 2(c). At $z_2 = 150$ mm, the main ring of the spot has started to recover. As shown in Fig. 2(d), the beam energy at the initial position is blocked by the obstacle, causing the energy of the side rings to flow from the surrounding area to the blocking area. When $z_2 = 250$ mm, a relatively high peak appears in the center of $x$-axis and a new spot begins to appear at the main ring position. As depicted in Fig. 2(f), with the increase in $z_2$, the number of peaks at the center of $x$-axis increases. Moreover, the FWHM of the self-healing process of CAB in free space decreases from 1.58 mm to 0.29 mm, which indicates the main ring has almost become a solid spot. When $z_2 = 625$ mm, the beam has basically reconstructed.

### 4.2. The propagation characteristics of CAB after the EIT-based light storage

The corresponding time sequence of the storage of CAB is shown in Fig. 3(a), Before the storage, the control beam is switched on in advance to prepare most of the atoms to the state $5S_{1/2}, F = 2$. The spatial intensity profile of the input probe beam is coded with CAB. We set the duration of the input probe beam as 1 μs. When the probe pulse completely enters the Rb vapor cell, the control beam is immediately turned off. The photon states carrying by the probe beam are transferred into atomic collective spin excitation and stored in the cell. After a programmable time delay of $\Delta T$, the control beam is switched on again to retrieve the probe pulse. In the meantime, the ICCD is activated by a trigger pulse to record the spatial intensity profile of the probe. In the experiment, we set the ICCD pulse duration with 6 μs to make sure that only the retrieved CAB signals can be collected.

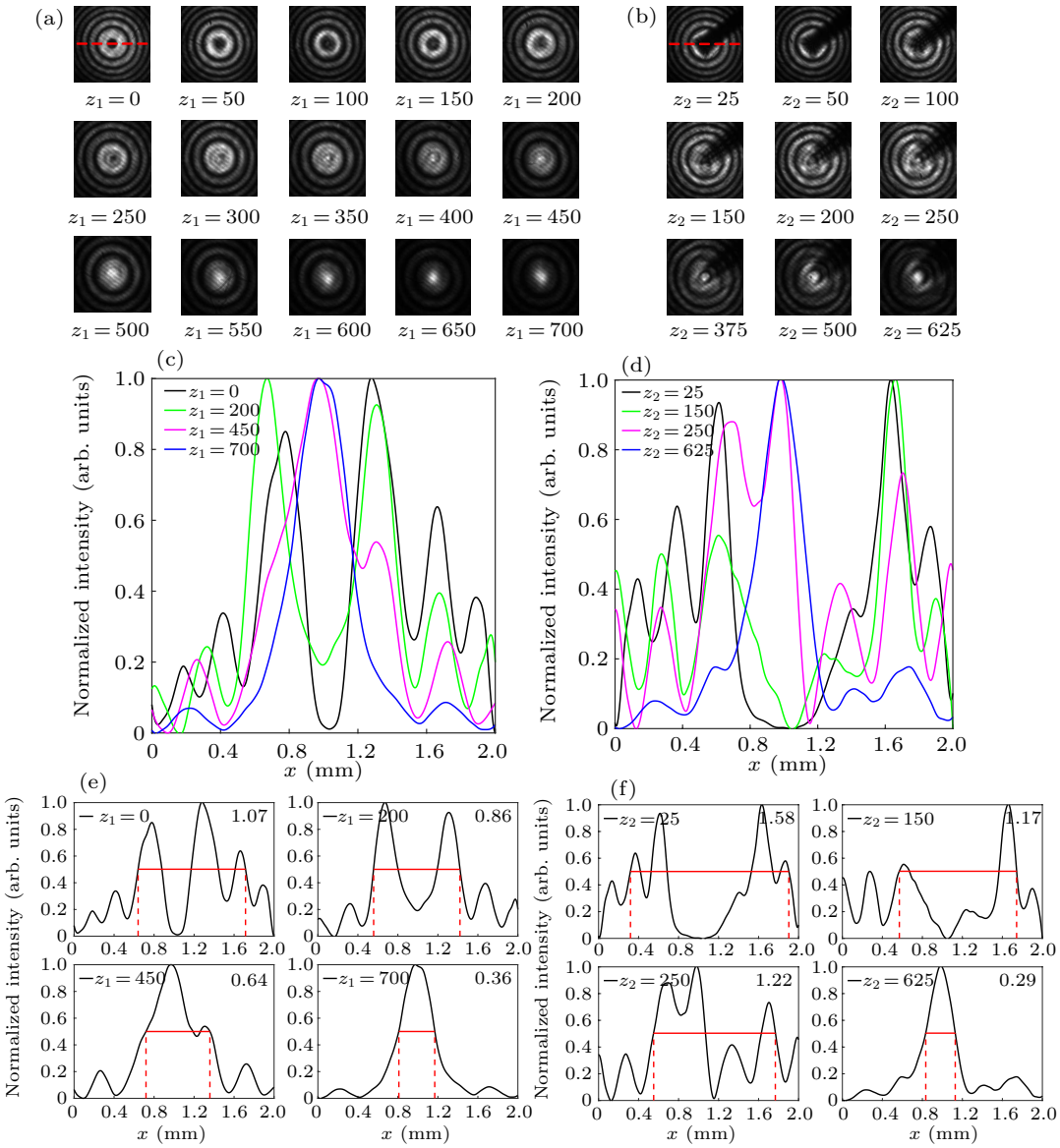



**Fig. 2.** (a) The autofocusing process of CAB in free space with different propagation distance $z_1$. (b) The self-healing process of CAB in free space with different propagation distance $z_2$ when most of the main ring is blocked. The normalized intensity distribution of (c) the autofocusing property and (d) the self-healing property of CAB. The normalized intensity distribution is calculated at the red dashed line of different images. The full width at half maximum (FWHM) of (e) the autofocusing process and (f) the self-healing process of CAB in free space under different propagation distances corresponding to (c) and (d), respectively.

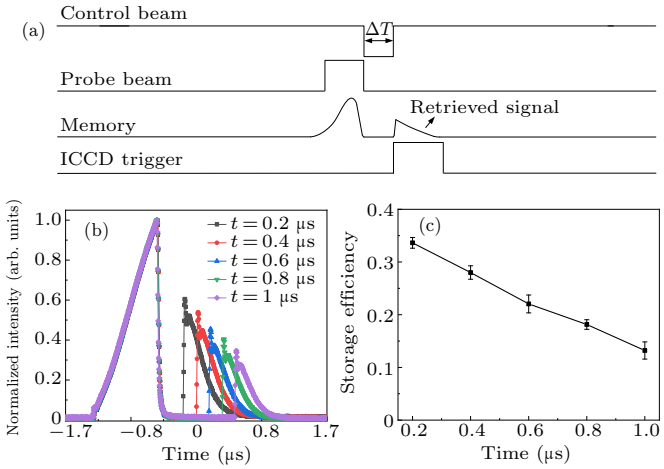



**Fig. 3.** (a) The time sequence of the storage of CAB. (b) The normalized intensities of CABs before storage and retrieved CABs after storage with different storage time $t$. (c) The storage efficiency of the light storage with different storage time $t$.

Figure 3(b) shows the normalized signal intensities before storage and after storage with different storage time $t$. When $t$ increases from 0.2 μs to 1 μs, the intensity of the retrieved CAB decreases, leading to a corresponding decrease of the storage efficiency from 0.34 to 0.13, as shown in Fig. 3(c).

To verify the property of the retrieved CAB, we investigate the autofocusing and self-healing process of the retrieved probe beam by changing $t$ and the distance of the ICCD during the propagation. Figure 4 shows the experimental results of the autofocusing process of the retrieved CAB after the EIT-based storage with the different $t$ and $z_1$, where $z_1$ is the distance between the plane of image and ICCD.

Figure 4(a) shows the intensity distribution of the spatial intensity profile of CAB recorded by ICCD. As the propagation distance increases, the CAB's power flows from the side

rings to the main ring, and turns to a circular bright spot. By comparing with the cases of different storage time $t$, we can investigate that the autofocusing property of CAB after storage remains even suffering from atomic diffusion. As shown in Fig. 4(b), when $t$ increases, the approximate profiles of the retrieved CABs remain. By fitting the data of the light field patterns at $z_1 = 700$ mm for different $t$ values, the intensity distribution curves of Fig. 4(b) can be obtained. The data in black, magenta, green, blue, and red correspond to $t$ reaching 0.2 μs, 0.4 μs, 0.6 μs, 0.8 μs, and 1 μs, respectively. As depicted in Fig. 4(b), the atomic diffusion with increasing storage time has a great influence on the spatial distribution of CAB, which can be seen from the FWHM. We used the similarity $S$ to quantitatively characterize the differences of the beam profiles. The real intensity distribution (not normalized) of the probe beam is used to calculate the value $S$, as presented in Tables 1 and 2. The expression of the similarity $S$ is[49,50]

$$S = \sum_m \sum_n A_{mn} B_{mn} \Big/ \sqrt{\left(\sum_m \sum_n A_{mn}^2\right)\left(\sum_m \sum_n B_{mn}^2\right)}, \qquad (3)$$

where $A$ and $B$ are the grey-scale matrices of the two images before and after storage. The $m$ and $n$ correspond to the coordinates, respectively. Herein, we calculate both the similarity $S_{\text{total}}$ of total CAB and the $S_{\text{main}}$ of its main ring. We select a square area of figures to calculate $S_{\text{main}}$ and the area's length and width are exactly tangent to the main ring. Furthermore, in our subsequent research, we will code the main ring with orbital angular momentum modes, which is useful for high-dimensional quantum information. Therefore, we focus on the evolution of the main ring of CAB. The similarities at different storage times ranging from 0.2 μs to 1 μs are illustrated in Table 1. As indicated by the $S_{\text{main}}$ values in Table 1 and the intensity profiles of CAB in Fig. 4(b), at the same position $z_1$, CAB's shape remains unchanged during the process.

As shown in Fig. 4(a), with increasing distance $z_1$ for the same storage time $t$, the width of the main ring becomes narrower and the side lobe energy becomes lower, which indicates that most of the side lobe energy flows to the main lobe. The CAB becomes a solid spot and focuses at $z_1 = 700$ mm.

**Table 1.** The $S$ against storage time $t$ at the same detection distance $z_1 = 700$ mm.

| $t$ (μs) | $S_{\text{total}}$ | $S_{\text{main}}$ |
|---|---|---|
| 0.2 | 0.86 | 0.95 |
| 0.4 | 0.81 | 0.93 |
| 0.6 | 0.78 | 0.92 |
| 0.8 | 0.76 | 0.90 |
| 1 | 0.76 | 0.87 |

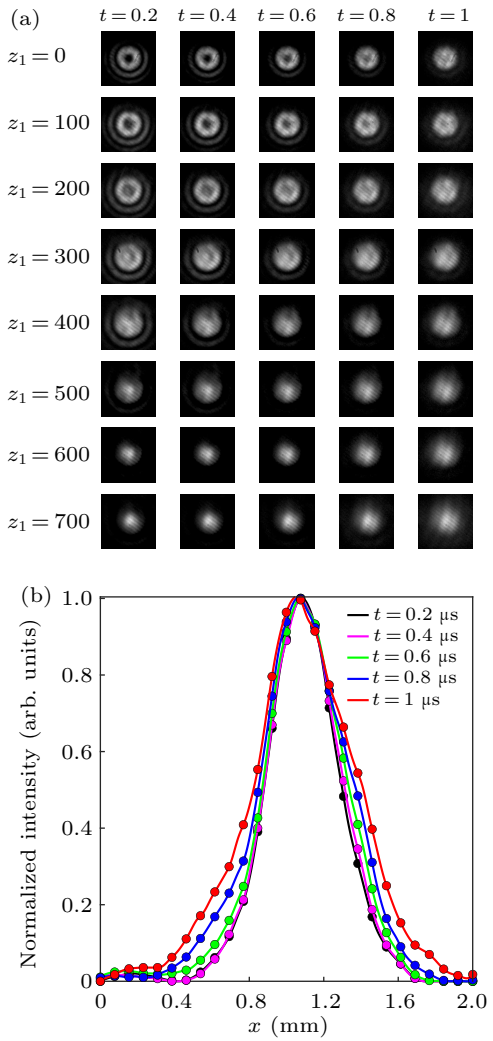



**Fig. 4.** (a) The autofocusing property of the retrieved CABs for different propagation distances $z_1$ and different storage time $t$. (b) The normalized intensity distribution of CAB with different storage time $t$ at the same detection distance $z_1 = 700$ mm.

We further investigate the self-healing effect of retrieved CAB. Figure 5 shows the experimental results of the self-healing process of the retrieved CAB for different $z_2$. As shown in Fig. 5, the energy of the secondary and other lobes flow to the main ring as the $z_2$ increases.

In the experiment, we use the same obstacle mentioned in 4.1 to block the main lobe, and observe the self-healing effect. It is clear to see that the main ring in the blocked area begins to be reborn at $z_2 = 150$ mm. Moreover, with the same storage time $t$ at the different $z_2$ in Fig. 5(a), the blocked area's light intensity increases, which means that the self-healing property of CAB can be maintained well after storage. Furthermore, when $z_2 = 375$ mm, the main ring of CAB gradually becomes a bright spot at the center, which also depicts the autofocusing characteristic of CAB after storage.

By fitting the data of the light field patterns at $z_2 = 625$ mm for different $t$ values, the intensity distribution curves of Fig. 5(b) can be obtained. The data in black, magenta, green, blue, and red correspond to $t$ reaching 0.2 μs, 0.4 μs, 0.6 μs, 0.8 μs, and 1 μs, respectively. When $t$ increases, the

diffusion of atoms greatly affects the spatial distribution of CAB, leading to different FWHM values in Fig. 5(b). The similarities under different storage times are depicted in Table 2. According to the $S_{\text{main}}$ values presented in Table 2 and the intensity profiles of CAB displayed in Fig. 5(b), at the same position $z_2$, CAB's shape remains unchanged during the propagation.

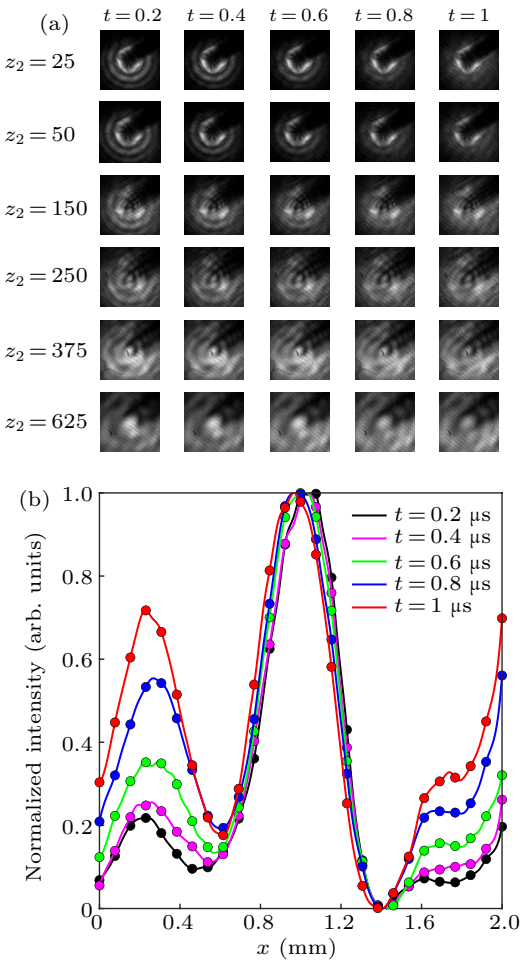



**Fig. 5.** (a) The self-healing property of the retrieved CABs with different storage time $t$ and different propagation distances $z_2$. (b) The normalized intensity distribution of CAB with different storage time $t$ at the same detection distance $z_2 = 625$ mm.

**Table 2.** The $S$ against storage time $t$ at the same detection distance $z_2 = 625$ mm.

| $t$ (μs) | $S_{\text{total}}$ | $S_{\text{main}}$ |
|---|---|---|
| 0.2 | 0.87 | 0.92 |
| 0.4 | 0.83 | 0.90 |
| 0.6 | 0.81 | 0.89 |
| 0.8 | 0.82 | 0.90 |
| 1 | 0.83 | 0.90 |

The above results illustrate that the properties of the retrieved CABs remain preserved as storage time $t$ increases, and the blocked parts are almost reborn after storage. The results further prove that the CAB can maintain its autofocusing and self-healing properties well after the storage process even suffering from atomic diffusion.

## 5. Conclusion and perspectives

In conclusion, we have investigated the propagation properties and the optical storage of CAB with the $\Lambda$-type EIT-based storage scheme in a hot atomic vapor. The probe beam is coded with CAB's wave packets in the transverse profile by using the SLM. The experimental results show that the autofocusing and self-healing effect of the retrieved CABs could be preserved well after storage. Furthermore, our research can be useful for high-dimensional spatial multi-modes storage. In addition, it also will play an important role in high-dimensional quantum communication to improve the channel capacities of quantum internet.

## Acknowledgement

Project supported by the Youth Innovation Promotion Association of Chinese Academy of Sciences.

## References

[1] Efremidis N K and Christodoulides D N 2010 *Opt. Lett.* **35** 4045
[2] Papazoglou D G, Efremidis N K, Christodoulides D N and Tzortzakis S 2011 *Opt. Lett.* **36** 1842
[3] Chremmos I, Zhang P, Prakash J, Efremidis N K, Christodoulides D N and Chen Z G 2011 *Opt. Lett.* **36** 3675
[4] Siviloglou G A and Christodoulides D N 2007 *Opt. Lett.* **32** 979
[5] Mohanty K, Mahajan S, Pinton G, Muller M and Jing Y 2018 *IEEE Trans. Ultrason. Ferroelectr. Freq. Control.* **65** 1460
[6] Jiang Y F, Cao Z L, Shao H H, Zheng W T, Zeng B X and Lu X H 2016 *Opt. Express* **24** 18072
[7] Lu W L, Sun X, Chen H J, Liu S Y and Lin Z F 2019 *Phys. Rev. A* **99** 013817
[8] Shahabadi V and Abdollahpour D 2021 *J. Quant. Spectrosc. Radiat. Trans.* **272** 107771
[9] Moradi H, Jabbarpour M, Abdollahpour D and Hajizadeh F 2022 *Opt. Lett.* **47** 4115
[10] Panagiotopoulos P, Papazoglou D G, Couairon A and Tzortzakis S 2013 *Nat. Commun.* **4** 2622
[11] Hang C and Huang G X 2014 *Phys. Rev. A* **89** 013821
[12] Wang J M, Zuo Y, Wang X C, Christodoulides D N, Siviloglou G A and Chen J F 2024 *Phys. Rev. Lett.* **132** 143601
[13] Efremidis N K, Paltoglou V and von Klitzing W 2013 *Phys. Rev. A* **87** 043637
[14] Goutsoulas M and Efremidis N K 2018 *Phys. Rev. A* **97** 063831
[15] Kadlimatti R and Parimi P V 2019 *IEEE Trans. Antennas Propag.* **67** 260
[16] Lai S T, Wang Y H, Lan Y P and Qian Y X 2019 *Ann Phys.* **531** 1900168
[17] Zheng G L, Wan L L, He T F, Wu Q Y and Zhang X H 2024 *Photonics* **11** 64
[18] Siviloglou G A, Broky J, Dogariu A and Christodoulides D N 2008 *Opt. Lett.* **33** 207
[19] Hu Y, Zhang P, Lou C B, Huang S, Xu J J and Chen Z G 2010 *Opt. Lett.* **35** 2260
[20] Ye Z Y, Liu S, Lou C B, Zhang P, Hu Y, Song D H, Zhao J L and Chen Z G 2011 *Opt. Lett.* **36** 3230
[21] Zhuang F, Shen J Q, Du X Y and Zhao D M 2012 *Opt. Lett.* **37** 3054
[22] Hang C and Huang G X 2013 *Phys. Rev. A* **88** 013825
[23] Ye F J, Zhang L Y, Wang F R, Yang Y M, Yu Y, Liu J, Wei D, Zhang P, Gao H and Li F L 2015 *Opt. Commun.* **345** 129
[24] Zhong H, Zhang Y Q, Zhang Z Y, Li C B, Zhang D, Zhang Y P and Belić M R 2016 *Opt. Lett.* **41** 5644
[25] Wu Z K, Zhang Q, Guo H and Gu Y Z 2018 *Optik* **164** 465
[26] Gong X S, Hua Y H and Wu Z K 2019 *Optik* **199** 163116
[27] Duan L M, Lukin M D, Cirac J I and Zoller P 2001 *Nature* **414** 413
[28] Phillips D F, Fleischhauer A, Mair A, Walsworth R L and Lukin M D 2001 *Phys. Rev. Lett.* **86** 783

[29] Fleischhauer M, Imamoglu A and Marangos J P 2005 *Rev. Mod. Phys.* **77** 633
[30] Yan Z H, Wu L, Jia X J, Liu Y H, Deng R J, Li S J, Wang H, Xie C D and Peng K C 2017 *Nat. Commun.* **8** 718
[31] Ma L X, Lei X, Yan J L, Li R Y, Chai T, Yan Z H, Jia X J, Xie C D and Peng K C 2022 *Nat. Commun.* **13** 2368
[32] Moiseev S A and Kröll S 2001 *Phys. Rev. Lett.* **87** 173601
[33] Moiseev S A and Tittel W 2011 *New J. Phys.* **13** 063035
[34] Guo J X, Feng X T, Yang P Y, Yu Z F, Chen L Q, Yuan C H and Zhang W P 2019 *Nat. Commun.* **10** 148
[35] Ding D S 2018 *Broad Bandwidth and High Dimensional Quantum Memory Based on Atomic Ensembles* (Singapore: Springer) pp. 91–107
[36] Hang C, Bai Z Y and Huang G X 2014 *Phys. Rev. A* **90** 023822
[37] Wang L, Sun Y H, Wang R, Zhang X J, Chen Y, Kang Z H, Wang H H and Gao J Y 2019 *Opt. Express* **27** 6370
[38] Wang C Y, Chen Y, Jiang Z B, Yu Y, Cao M T, Wei D, Gao H and Li F L 2022 *Front. Phys.* **17** 22503
[39] Yang X J and Wu Z S 2018 12*th International Symposium on Antennas, Propagation and EM Theory (ISAPE)*, December 3–6, 2018, Hangzhou, China, p. 1
[40] Li H, Liu H G and Chen X F 2018 *Opt. Express* **26** 21204
[41] Wei B Y, Liu S, Chen P, Qi S X, Zhang Y, Hu W, Lu Y Q and Zhao J L 2018 *Appl. Phys. Lett.* **112** 121101
[42] Liu X Y, Sun C and Deng D M 2021 *Chin. Phys. B* **30** 024202
[43] Huang Y H, Li X P, Akram Z, Zhu H and Qi Z H 2021 *IEEE Antennas Wirel. Propag. Lett.* **20** 1093
[44] Wang D M, Jin L W, Rosales-Guzmán C and Gao W 2021 *Appl. Phys. B* **127** 22
[45] Chen L, Wen J S, Sun D and Wang L G 2020 *Opt. Express* **28** 36516
[46] Abramowitz M and Stegun I A 1972 *Handbook of Mathematical Functions: with Formulas, Graphs, and Mathematical Tables* 10th edn. (Washington: U. S. National Bureau of Standards) pp. 446–448
[47] Li N, Jiang Y F, Huang K K and Lu X H 2014 *Opt. Express* **22** 22847
[48] Siviloglou G A, Broky J, Dogariu A and Christodoulides D N 2007 *Phys. Rev. Lett.* **99** 213901
[49] Glorieux Q, Clark J B, Marino A M, Zhou Z F and Lett P D 2012 *Opt. Express* **20** 12350
[50] Ding D S, Zhou Z Y, Shi B S and Guo G C 2013 *Nat. Commun.* **4** 2527